JOURNAL OF CATALYSIS 73, 337–348 (1982)

Mercury Removal from Waste Gases by Manganese Oxide Acceptors

S. CAVALLARO, N. BERTUCCIO, P. ANTONUCCI, AND N. GIORDANO

Istituto di Chimica Industriale, Università di Messina, Messina, Italy

AND

J. C. J. BART

Montedison "G. Donegani" Research Laboratories, Via G. Fauser 4, Novara, Italy

Received July 7, 1980; revised May 12, 1981

Removal of mercury vapour from a waste gas has been investigated at atmospheric pressure and at ambient temperature using a series of manganese-based reagents supported on an inert medium. The effect of catalyst composition on activity and the influence of relative humidity of the air stream have been studied. Whereas γ-Al_2O_3 has a very low mercury sorption capacity, sorption occurs copiously on impregnated silver- and copper-doped MnO_2 acceptors but the much higher activity is reduced by the presence of water vapour in the carrier gas. The morphological and microstructural characterization of the (MnO_2, $AgNO_3$) · γ-Al_2O_3 reagents has shown selective deposition of $AgNO_3$ particles on β-MnO_2 crystallites which are dispersed on the γ-Al_2O_3 matrix. As the adsorption is associated with a sequence of specific colour changes a chemical oxidation mechanism is proposed. Acceptor deactivation is discussed.

INTRODUCTION

Apart from its toxic, contaminative, and corrosive properties, traces of mercury poison many industrial catalytic processes, due to formation of stable bonds with the catalyst components. Therefore, purification of raw materials from mercury (e.g., moist hydrogen from electrolytic cells for hydrogenation, natural gas, etc.) or elimination of Hg as a by-product is highly desirable. Removal of mercury can be achieved either by physical adsorption on a molecular sieve or by chemical oxidation (*1–6*) and is usually performed at temperatures differing from room temperature. In this paper we report on the sorptive properties of several manganese-based materials towards Hg vapour. As a lead in this research we have taken the findings of Alekseevskii and co-workers (*7–11*) concerning the use of MnO_2 in Hg sorption. In particular, the effects of addition of Ag^+ and Cu^+ on the morphological and microstructural properties of β-MnO_2 supported on γ-Al_2O_3 are examined and the active sites of the chemisorption process are discussed.

EXPERIMENTAL

Reagents and Acceptors

Normal commercial-grade γ-Al_2O_3 (Pechiney St. Gobain) was calcined in air at 600°C for 1 h before use (BET surface area, 238 m^2/g). The acceptors investigated consisted of doped MnO_2/γ-Al_2O_3, prepared by "dry impregnation" of precalcined alumina of known pore volume with an equivalent volume of a solution (d = 1.54 g ml^{-1}) of $Mn(NO_3)_2$ (eventually in the presence of other cations), followed by drying in air at 110°C and activation at 190°C both for 24 h (Table 1). The colour of all finished samples ranged from pale tan to black. Since characterization of supported manganese oxides is difficult, the preparation technique was carefully standardized as the best means for providing comparable results.

0021-9517/82/020337-12$02.00/0

TABLE 1

Catalyst Preparation

Experiment	Al_2O_3 (g)	$Mn(NO_3)_2$ sol 50% (ml)	$AgNO_3$ (g)	$Cu(NO_3)_2$ (g)	$KMnO_4$ (g)	Total volume[a] (ml)	Temperature of drying and calcination (24 h) (°C)	BET surface area (m^2/g)
1	97.2	10.6	0.39	—	—	39.9	110–190	143.3
2	94.5	21.6	0.79	—	—	38.7	110–190	141.8
3, 5, 7, 8	91.5	32.6	1.26	—	—	37.5	110–190	138.6
4[b]	87.9	46.5	3.73	—	—	2 × 36.0	110–190	125.0
6	91.5	32.6	—	2.4	—	37.5	110–190	138.9
9	99.2	—	1.26	—	—	40.7	110–190	n.d.
10	20.0	—	—	—	—	—	110–190	238.0
11, 12	92.3	32.6	—	—	—	37.8	110–190	n.d.
13	99.0	—	—	—	1.0	40.6	60	n.d.
14	97.5	—	—	—	2.5	40.0	60	n.d.

[a] Equivalent to total pore volume.
[b] Double impregnation.

Dopants were added to the $Mn(NO_3)_2$ solution in the form of $Cu(NO_3)_2$ and $AgNO_3$.

The active oxygen content of the acceptors was determined by iodometric titration. One gram of the catalyst was dried at 110°C for 24 h and added to 50 ml H_2O, 1 ml glacial acetic acid, and 1 g KI in inert atmosphere. After 150 h the solution was titrated with sodium thiosulphate and starch amide as an indicator. The results are reported in Table 2, where the active oxygen content is expressed as the Mn^{4+}-ion fraction.

Apparatus

Figure 1 shows a diagram of the apparatus for Hg sorption measurements designed to provide carrier gas streams containing up to 10,000 μg Hg/m^3 at room temperature and atmospheric pressure for 0–70% relative humidity. The setup consists of a flowmeter (F & P Precision Bore Flowrater), a mercury reservoir, a 300-ml Pyrex vessel for admixing Hg vapour and the transport gas (dry or moist air), and a Pyrex glass adsorption column. The Hg vapour concentration was regulated by varying the flow rate and was normally set at 2500 μg/m^3. The carrier gas, prior to admixing with Hg, was either washed and humidified up to 70% relative humidity or dried over molecular sieves. No attempts were made to remove the heat of adsorption of water from the adsorption bed. The adsorption column was designed so that the ratio of the diameter of the adsorbent particles to column diameter was in the range $\frac{1}{7}$–$\frac{1}{10}$; the linear gas flow rate through the adsorption bed never exceeded 700 m h^{-1}.

Provision was made for sampling the gas

TABLE 2

Manganese Valence State in Various MnO_2/γ-Al_2O_3 Sorbents

Catalyst[a]	$Mn^{4+}/(Mn^{3+} + Mn^{4+})$ (%)
2.5 wt% Mn	24.0
5.0 wt% Mn	81.7
7.7 wt% Mn	81.7
11.0 wt% Mn	82.1
2.5 wt% Mn + 0.25 wt% Ag	74.3
5.0 wt% Mn + 0.5 wt% Ag	73.7
7.7 wt% Mn + 0.8 wt% Ag	78.3
9.0 wt% Mn + 0.9 wt% Ag	83.8
11.0 wt% Mn + 2.2 wt% Ag	84.5
7.7 wt% Mn + 0.8 wt% Cu	89.4

[a] Carrier: γ-Al_2O_3.

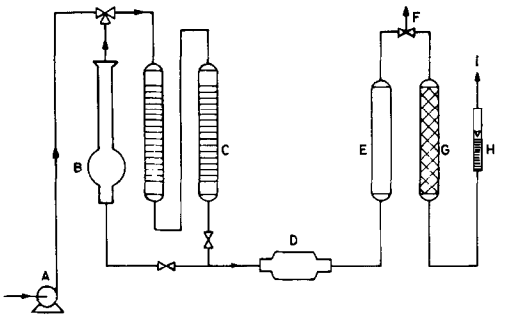

FIG. 1. Flow diagram of apparatus used for mercury sorption measurements consisting of pump, A; humidifier, B; desiccators, C; mercury reservoir, D; gas mixer vessel, E; adsorption column, G; and rotameter, H. The gas stream is analysed before (F) and after (I) the reaction.

stream by colorimetry using a Bausch & Lomb Spectronic 20 spectrophotometer. Analysis of this stream before and after reaction was performed each 72 and 24 h, respectively. The breakthrough point was determined as the instant in which the output reaction mixture contained more than 100 μg Hg/m^3.

Chemical Analysis

In view of the need to determine Hg in gaseous mixtures with a minimum concentration of about 0.2 mg/m^3 with a precision of better than 5%, classical analytical methods such as condensation of Hg vapour by cooling, amalgamation with metals (Au, Ag, Cu, Zn), and others (*12*) could not be applied and a procedure taken from air pollution studies (*13*) was slightly modified. In this method Hg is determined colorimetrically in the form of a diphenylthiocarbazone–mercury (II) complex (*14*). The gaseous mixture is passed through an acidified $KMnO_4$ solution which oxidizes Hg(0) to Hg(II). Under the reaction conditions employed, no restrictions are imposed on the Hg concentration. However, an upper limit of 200 liters h^{-1} was set to the flow rate of the gaseous mixture in order to absorb the mercury in 250 cm^3 $KMnO_4$ solution. After reduction of excess $KMnO_4$ with (excess) hydroxylamine sulphate or chlorohydrate at room temperature, mercury is extracted from the colourless solution by means of dithizone in $CHCl_3$ (0.001 wt%). Whereas the lower limit of $KMnO_4$ concentration and acidity for quantitative Hg uptake are 0.5 *M* $KMnO_4$ and 1.0 *M* H_2SO_4 (*15*), the upper limit of [$KMnO_4$] depends upon the maximum Mn^{2+}/Hg^{2+} ratio at which Hg^{2+} and Mn^{2+} ions are still separated by subsequent dithizone extraction. Thus, as mercury dithizonate is stable in highly acidic solutions, in contrast to the Mn^{2+} complex which dissociates under these conditions, Hg^{2+} may be extracted selectively from a 1 *M* acidic solution of high Mn^{2+} concentration (up to $Mn^{2+}/Hg^{2+} = 10^4$). The orange-coloured Hg^{2+} complex obtained, which absorbs at λ_{max} = 500 nm, is determined colorimetrically by comparison with standard mixtures. As $Hg(thi)_2$ is sensitive to air and light, a stabilizing agent (CH_3COOH, 6 *M*) was used.

Physicochemical Characterization

Batches of the samples were analysed by various techniques, as indicated below. Surface areas were calculated from the amount of N_2 absorbed from a N_2 + He stream, at liquid nitrogen temperature (*16*). Morphological and textural properties of the acceptors were studied by transmission electron microscopy (TEM), using a Philips 300 EM up to 245,000× magnification. Samples for TEM were prepared by the extractive replica technique (*17*). After deposition of carbon on the finely dispersed specimen, the sample was leached with a 0.8-wt% solution of HF. As a result, part of the supported material was separated from the carrier and adhered to the carbon film. This replica was then examined. In the case of Cu-containing samples, leaching with HF was much reduced in order to prevent dissolution of the copper particles.

X-Ray powder techniques (Philips 1050/1070 setup; Cu$K\alpha$ radiation) were used for phase identification; diffraction patterns were compared to the standards of

TABLE 3

Mercury Sorption of Various Reagents

Run	Active phase[a]	Air flow rate (liter h^{-1})	Space velocity (h^{-1})	Relative humidity (%)	Mean Hg feed concn ($\mu g/m^3$)	Catalyst weight (g)	Breakthrough time (h)	Catalyst efficiency	
								(g Hg/kg catalyst)	(mg Hg/g Mn)
1	2.5 wt% Mn + 0.25 wt% Ag	40	2000	70	2.800	20	70	0.39	15.6
2	5.0 wt% Mn + 0.5 wt% Ag	40	2000	70	2.450	20	320	1.57	31.4
3	7.7 wt% Mn + 0.8 wt% Ag	40	2000	70	2.330	20	1040	4.84	62.9
4	11.0 wt% Mn + 1.1 wt% Ag	40	2000	70	2.700	20	1750	9.45	85.9
5	7.7 wt% Mn + 0.8 wt% Ag	40	2000	0	3.100	20	1100	6.82	88.6
6	7.7 wt% Mn + 0.8 wt% Cu	40	2000	70	3.100	20	1150	7.13	92.6
7	ex run 5[b]	40	2000	0	4.700	20	0	0	0
8	ex run 7[c]	40	2000	0	4.700	20	0	0	0
9	0.8 wt% Ag	40	2000	70	3.870	20	300	2.32	—
10	None	40	2000	70	3.150	20	0	0	—
11	7.7 wt% Mn	108	1200	0	1.140	50	370	0.91	11.8
12	7.7 wt% Mn	108	2000	70	1.200	50	100	0.26	3.4
13	0.35 wt% Mn	40	2000	70	1.000	20	750	1.50	428.6
14	0.87 wt% Mn	40	2000	70	1.000	20	2250	4.50	517.2

[a] For catalyst preparation, see Table 1. Carrier: γ-Al_2O_3. Composition in cation fractions.
[b] After exposure to air for 30 days at room temperature.
[c] After grinding.

the various MnO_2 polymorphs (ASTM 7-222, 12-141, 12-714, 12-716, 14-644, 18-802), Ag (ASTM 4-783), AgO (ASTM 14-646 and 22-472), Ag_2O (ASTM 12-793), $AgNO_3$ (ASTM 6-363), $AgNO_2$ (ASTM 6-349), and γ-Al_2O_3 (ASTM 10-425). Differential thermal analysis (DTA), using a Mettler TA2 thermoanalyzer, was employed to examine the thermal properties of $AgNO_3$ and $Mn(NO_3)_2 \cdot 6H_2O$. The NO_3^- concentration of the catalyst was determined after reduction by elemental Kjeldahl analysis of N.

RESULTS

Mercury Adsorption Experiments

The breakthrough time and efficiency of various sorbents in Hg uptake have been determined experimentally in the apparatus described above. All runs were performed in a standard fashion at room temperature, using a constant space velocity of about 2000 h^{-1}. In typical experiments the sorbent (20 g) was exposed to a stream of moist air (70% relative humidity; flow rate, 40 liters h^{-1}) containing variable amounts of Hg. Operating details and results of various acceptors are collected in Table 3. Results of a series of Hg sorption experiments, performed on Al_2O_3-supported $KMnO_4$, are also given. Results reported in Figs. 2 and 3 show the demercurization over various adsorbents as a function of the time on stream. Working capacity or catalyst efficiencies under the particular conditions of mercury feed concentration (Table 3) were calculated from the breakthrough times assuming that all the mercury delivered to a column up to the breakthrough point was adsorbed by the sorbent. After reaching equilibrium conditions at the adsorption bed ($[Hg]^{effluent} = [Hg]^{feed}$) experiments were discontinued. As is evident from Table 3 and Figs. 2 and 3 the breakthrough times vary with the catalyst composition whereas the catalytic efficiency of the sorbents at equilibrium (saturation) follows the order of breakthrough time. It was also observed that the MnO_2/γ-Al_2O_3 sorbent, initially black in colour, changed slowly to white-spotted black during each run.

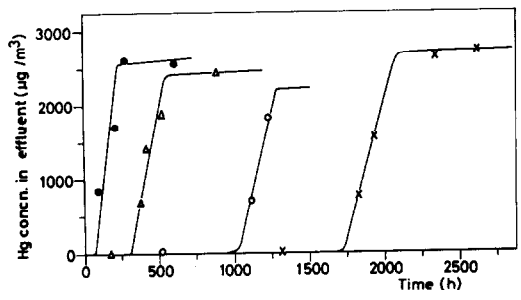

FIG. 2. Performance of Al_2O_3 + 2.5 wt% Mn + 0.25 wt% Ag^+ (●), Al_2O_3 + 5.0 wt% Mn + 0.5 wt% Ag^+ (△), Al_2O_3 + 7.7 wt% Mn + 0.8 wt% Ag^+ (○), Al_2O_3 + 11.0 wt% Mn + 2.2 wt% Ag^+ (×) in mercury sorption (in $\mu g/m^3$). Carrier gas: moist air (70% relative humidity).

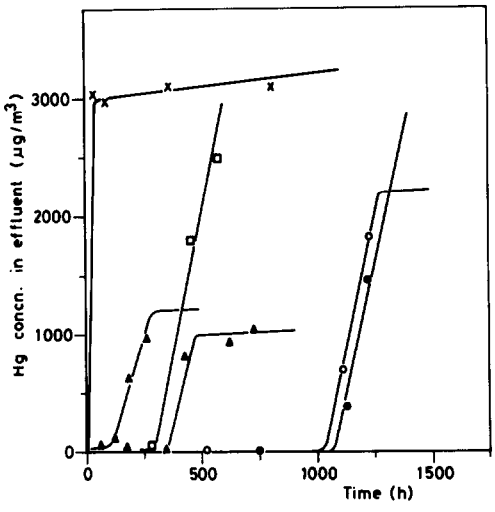

FIG. 3. Mercury sorption (in $\mu g/m^3$) on Al_2O_3 in moist air (×), Al_2O_3 + 0.8 wt% Ag in moist air (□), Al_2O_3 + 7.7 wt% Mn in dry air (△) and in moist air (▲), Al_2O_3 + 7.7 wt% Mn + 0.8 wt% Ag^+ in moist air (○) and in dry air (●).

Phase Distribution and Morphology

Samples of MnO_2 (C. Erba), freshly prepared β-MnO_2/γ-Al_2O_3, $AgNO_3/\gamma$-Al_2O_3, and (β-MnO_2 + $AgNO_3$)/γ-Al_2O_3 sorbents with varying compositions (up to 11 wt% Mn and 10 wt% Ag), and the corresponding Hg-saturated catalysts were studied by

TEM to investigate the nature of the active sites for the mercury adsorption. Three phases were distinguished in the sorbent samples: γ-Al_2O_3, β-MnO_2, and $AgNO_3$.

In the case of alumina-supported $AgNO_3$, the nonidiomorphic nature of γ-Al_2O_3 was clearly visible with its mean fine grain size of about 1 μm. Silver-containing particles were present as homogeneously distributed, well-rounded, solidified drops (mean diameter ranging from 50 to 300 Å in 1 wt% $AgNO_3$ and from 50 to 1400 Å in 10 wt% $AgNO_3$ on Al_2O_3); they appear dark in the image. The chemical nature of these particles is easily determined if we consider that $AgNO_3$ shows a phase transition at 156°C and melts at 205°C, i.e., close to the calcination temperature of the catalyst samples. As degradation of pure $AgNO_3$ to $AgNO_2$ sets in at 455°C (*18*) and Ag_2O and Ag are formed only at about 350°C in 10% $AgNO_3/Al_2O_3$, it is to be expected that at the temperatures used in the present experiments silver ions are in nitrate form, in accordance with chemical analysis (10 wt% Ag/Al_2O_3: $(NO_3)^-$ obsd, 4.62 wt%; calcd, 5.75 wt%).

Alumina-based manganese oxide samples consist of clusters of β-MnO_2 particles with idiomorphic tendency, varying greatly in crystalline size (up to 3 μm) and contrasting with the smaller γ-Al_2O_3 particles. The texture of fresh and spent doped MnO_2 sorbents on alumina differs fundamentally from that in the absence of the dopants (Ag^+ or Cu^+). As mentioned above, in $AgNO_3 \cdot \gamma$-Al_2O_3 the supported phase is uniformly distributed on the carrier; instead, in (β-MnO_2 + $AgNO_3$)/γ-Al_2O_3 (up to 11 wt% Mn and 2 wt% Ag), the $AgNO_3$ droplets are selectively concentrated along the borders of the idiomorphic MnO_2 aggregates and on top of the particles (Figs. 4–6). Apparently, γ-Al_2O_3 acts as a true support

FIG. 4. Microphotograph of Al_2O_3 loaded with 7.7% Mn and doped with 0.8% Ag after sorption of 128,000 μg Hg. $AgNO_3$ particles are located selectively on β-MnO_2 dispersed in γ-Al_2O_3.

FIG. 5. Microphotograph of Al_2O_3 loaded with 7.7% Mn and doped with 0.8% Ag after Hg sorption.

for MnO_2 with $AgNO_3$ being dispersed onto the latter only. It is not surprising to find that at higher loadings (10 wt% Ag) $AgNO_3$ particles also accumulate onto γ-Al_2O_3, initially as fines (much smaller than the particles dispersed on MnO_2) and as agglomerates in the richest samples. Activation of the reagents in an inert atmosphere leads to dispersion of Ag particles over γ-Al_2O_3, even at such low loads as 0.5 wt% $AgNO_3$. This is at variance with the structure of the catalysts prepared in air or in an O_2 atmosphere and seems to indicate a much stronger interaction between Ag^+ and MnO_2 in the latter case.

Doping of MnO_2/γ-Al_2O_3 with Cu ions causes drastic structural and textural changes in the solid through chemical interaction; these effects are clearly illustrated by Fig. 7, especially if compared to Figs. 4–6 for the analogous Ag samples. It appears that the porosity of the original allotriomorphic γ-Al_2O_3 increases on addition of Cu ions.

The result of X-ray diffraction measurements are in agreement with the optical observations. (MnO_2 + $AgNO_3$)/γ-Al_2O_3 samples are essentially amorphous or microcrystalline but characteristic d spacings of β-MnO_2 (pyrolusite, ASTM 12-716; a = 4.40, c = 2.87 Å) are present in the samples containing more than 2.5 wt% Mn. This result differs from Alekseevskii's findings, which were formerly criticized by Moore *et al.* (*19*). Namely, thermal decomposition of $Mn(NO_3)_2 \cdot 6H_2O$ usually leads to β-MnO_2 (*19, 20*), although either β- or γ-MnO_2 may be formed in the presence of other cations (*21*). β-MnO_2 was also found in the Ag- and Cu-doped samples. Nevertheless, although MnO_2 is present in its most well defined crystalline form, results of Table 2 show nonstoichiometry, as usual (*22*). No indications were found for products of interaction

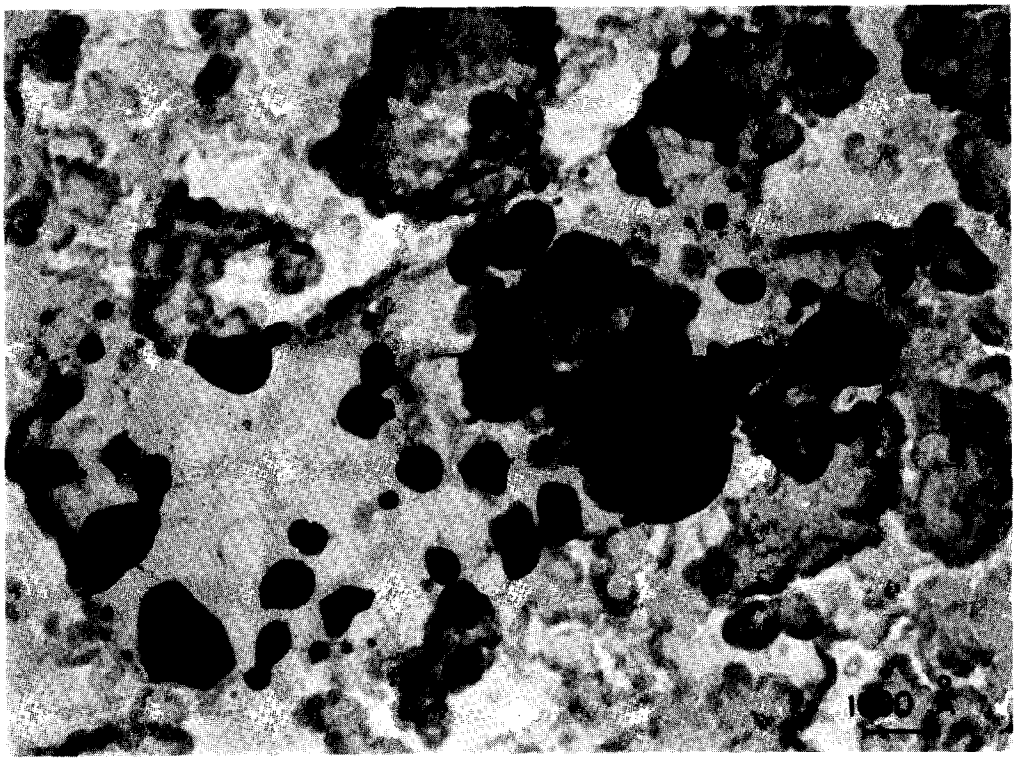

FIG. 6. Microphotograph of Al_2O_3 loaded with 7.7% Mn and doped with 0.8% Ag after Hg sorption.

between γ-Al_2O_3 and MnO_2. The small γ-Al_2O_3 particles give rise to diffuse reflections, and no diffraction bands corresponding to $AgNO_3$ or other silver species were observed. This even holds for γ-Al_2O_3 loaded with up to 10 wt% Ag, indicating either solidification of molten $AgNO_3$ without rearrangement to a regular crystal lattice or very small crystallite size of ordered $AgNO_3$ particles. Fresh and spent catalysts show identical X-ray powder diffraction patterns.

DISCUSSION

Activity of Undoped Samples in Dry Air

The experiments establish that pure γ-Al_2O_3 has no Hg sorption capacity in contrast to supported silver compounds (runs 9 and 10 of Table 3, cf. also Fig. 3), which exhibit low activity. In the latter case it may be envisaged that Hg sorption proceeds by chemisorptive reduction of Ag^+, as for uptake of Hg vapour by silver-zeolites (*6*). Even so, no metallic silver was detected by X-ray diffraction. The poor performance of the MnO_2/γ-Al_2O_3 acceptor in dry air as compared to doped samples (cf. runs 5 and 11 of Table 3) must be considered in relation to the fact that in the former case the active material is present as relatively large crystals according to XRD and TEM.

As mentioned above, according to Alekseevskii and co-workers (*7–11*), MnO_2 shows the highest Hg sorptive properties among a variety of materials. This has been attributed to the high oxidation power of Mn^{4+}, known from oxidation reactions of CO, SO_2, aniline, etc. (*23–27*). According to the Russian work, the activity of the various MnO_2 modifications varies as $\alpha \gg \gamma \gg \beta \simeq 0$. In the absence of the α and γ forms, our results definitely indicate very

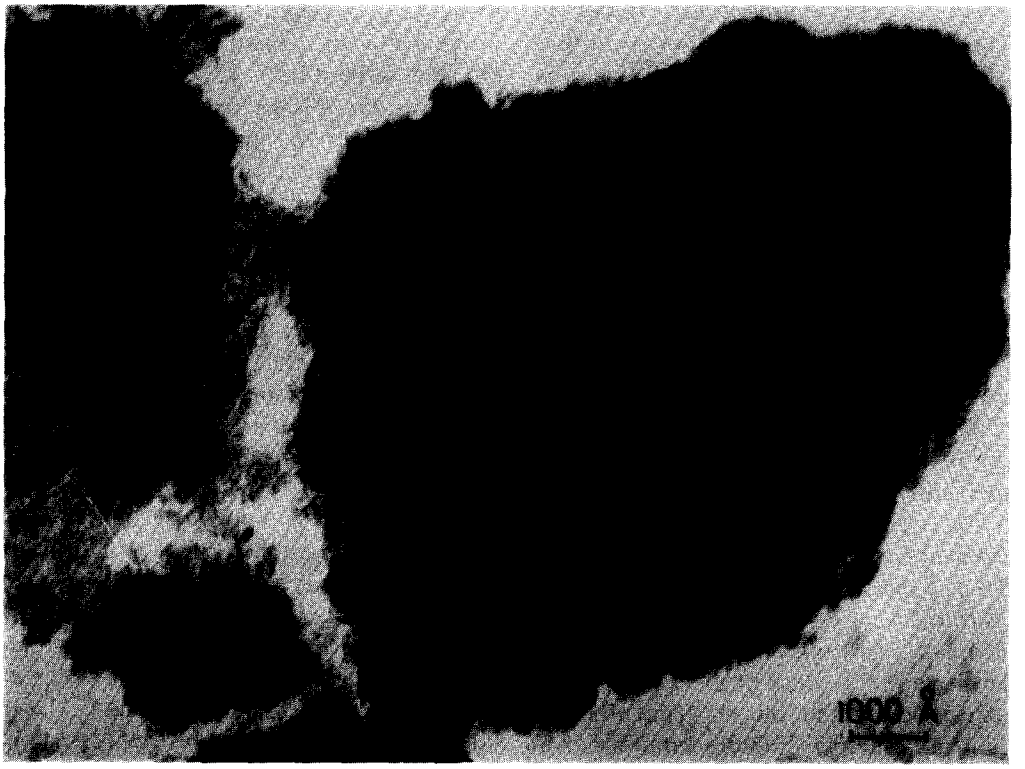

FIG. 7. Microphotograph of Al_2O_3 loaded with 5% Mn and doped with 3% Cu.

poor catalytic activity for the nonstoichiometric β form, at least in undoped samples. On the other hand, it is also well known that stoichiometric MnO_2 is not an active oxidation catalyst (*28*). The oxidizing properties of MnO_2 are determined by the presence of oxygen dissociatively chemisorbed on the surface. This chemisorbed oxygen also most probably accounts for the surface excess oxygen determined by the KI method. It is worthy of mention that there actually appear to be two kinds of active oxygen present in MnO_2, of which only one plays a role in the oxidation reaction of CO to CO_2 (*29–31*). This finding may be correlated with the fact that manganese nodules are known to adsorb cations such as Ag and Co only at pH > 8, i.e., in oceanic rather than sweet-water basins (pH < 7). These facts are obviously related to the zero point of charge (z.p.c.) of the metallic oxide. The observations agree with our findings showing that use of SiO_2 as a support instead of Al_2O_3 results in an inactive catalyst.

With regard to the MnO_2/γ-Al_2O_3 system, very little information is available as to the nature of the interaction between the components. Impregnation of γ-Al_2O_3 with $Mn(NO_3)_2$ results in a very weak interaction between the carrier and the Mn oxide obtained after calcination (*32*). As a matter of fact, in accordance with the observations of Selwood *et al.* concerning γ-Al_2O_3-supported $Mn(NO_3)_2$ catalysts (*20*), our results show that the layer of manganese oxide in the pyrolusite structure contains a considerable fraction of Mn^{3+} cations, especially at low Mn concentrations. The presence of Mn^{3+} may be explained by valence inductivity, i.e., the tendency of manganese oxide to imitate the crystal structure of the support, even to the extent of changing the oxidation state (*20*). In this respect, it is

relevant to observe that γ-Mn_2O_3 and γ-Al_2O_3 are isomorphous substances. From the Mn^{3+}/Mn^{4+} distribution in the various catalysts (Table 2), it appears that neither Mn^{4+} nor Mn^{3+} ions are catalytically active sites in the MnO_2 oxidation of Hg and of the other molecules mentioned above.

Role of Promoters

In moist air, as well as in N_2, MnO_2/γ-Al_2O_3 is also almost inactive (run 12 of Table 3, cf. also Fig. 3). In accordance with the observations of Katz (*33*), doping with Ag^+ and Cu^{2+} cations greatly enhances adsorption with respect to MnO_2/γ-Al_2O_3, independently of the Mn level (Table 3). The activity is slightly greater under dry than under wet conditions (cf. Fig. 3 and runs 3 and 5 of Table 3). This is in line with results of chromic acid on silica (*5*), where water molecules are strongly adsorbed by the sorbent preventing access of mercury. It is to be noticed that under our experimental conditions the samples rapidly equilibrate at 70% relative humidity. The water molecules in the MnO_2 matrix are present as H_2O or H_3O^+ (*34*).

As to the promoting action, it should be recalled that doping of a MnO_2 catalyst with Ag ions positively affects oxidation of acetylene (*35*) and overcomes the poisoning by water, thus improving the catalyst lifetime. Unpromoted Hopcalite catalysts (60% MnO_2 + 40% CuO), which are rapidly spent in a flow of moist air containing 5 ppm of acetylene at a space velocity of 10^5 h^{-1} at 150°C, are stabilized after addition of 10% Ag_2O and show better performance than Ag_2O/Al_2O_3 catalysts. Even better results are obtained for $(MnO_2 + AgMnO_4)/Al_2O_3$ catalysts. Similarly, Katz and Halpern (*36*) report effective oxidation of CO in air at room temperature using a $AgMnO_4$ catalyst in the presence of metallic oxides. The reason for the promoting effect of CuO in MnO_2–CuO catalysts has also been discussed in terms of compound formation, namely, of $CuMn_2O_4$ (*28*). It is equally of interest to notice our results obtained by using $KMnO_4$-based catalysts. As shown in Table 3 and Figs. 8 and 9, $KMnO_4$ is a most efficient sorbent (runs 13 and 14 of Table 3). We consider this as another argument in favour of active species different from Mn^{4+}. It then appears reasonable to tie the effective action of Ag-doped β-MnO_2/γ-Al_2O_3 sorbents to the presence of such MnO_4^- ions. As is well known, Ag^+ catalyses the oxidation of Mn^{4+} to Mn^{7+} (*37*), even though the experimental conditions for such a process differ from ours and require higher temperatures. However, at solid surfaces reaction conditions often differ considerably from those in the liquid phase.

The chemical topology, as observed on the microphotographs, indicates a high degree of selectivity of $AgNO_3$ with regard to the components of the system (β-MnO_2 and γ-Al_2O_3). Apparently, $AgNO_3$ nuclei preferentially settle on the MnO_2 surface, suggesting loci of chemical interaction. The resulting surface coverage of MnO_2 particles as a consequence of the high mobility of the low-melting $AgNO_3$ provides a reasonable explanation for the promoting effects of small amounts of $AgNO_3$ on the sorption properties. It remains to be seen whether silver participates in the chemisorption process in the form of $AgMnO_4$ or whether it just promotes formation of MnO_4^-. Formation of $AgMnO_4$ is appealing in view of

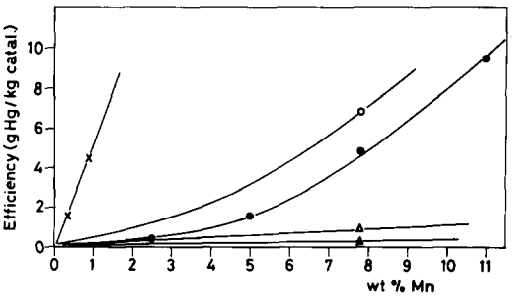

FIG. 8. Catalyst efficiency (g Hg/kg catalyst) vs weight percentage of Mn: Al_2O_3 + MnO_2 (undoped) in dry air (△), Al_2O_3 + MnO_2 (Ag doped) in moist air (●), Al_2O_3 + MnO_2 (undoped) in moist air (▲), Al_2O_3 + MnO_2 (Cu doped) in moist air (○), Al_2O_3 + $KMnO_4$ in moist air (×).

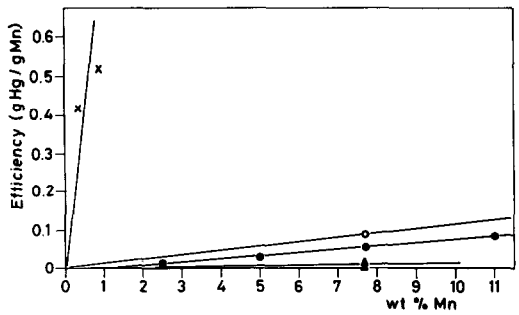

FIG. 9. Catalyst efficiency (g Hg/g Mn) vs weight percentage of Mn: Al_2O_3 + MnO_2 (undoped) in dry air (△), Al_2O_3 + MnO_2 (Ag doped) in moist air (●), Al_2O_3 + MnO_2 (undoped) in moist air (▲), Al_2O_3 + MnO_2 (Cu doped) in moist air (○), Al_2O_3 + $KMnO_4$ in moist air (×).

the great chemical inertness of alumina and the unfavourable conditions for interaction between MnO_2 and Al_2O_3. However, pure $AgMnO_4$ is not stable under the conditions of calcination employed in our experiments. Examination of the granule surface after Hg sorption shows that the particles have withstood the reaction virtually unchanged, apart from a colour change, probably indicative of the formation of surface compounds. Reactions such as

$$AgMnO_4 + 2Hg \rightarrow MnO_2 + Ag + 2HgO$$

would certainly proceed beyond surface modification of the granules and eventually lead to crumbling of the structure. The Hg sorption by the granular reagents thus probably involves a truly catalytic oxidation reaction with oxygen of the bulk gas phase. As no differences in morphology and X-ray phase distribution were noticed on fresh and spent samples, no direct information is available on the interaction of mercury with its sorbents. In particular, we are not in a position to confirm the amalgamation

$$Hg + MnO_2 \rightarrow HgMnO_2$$

according to Ref. (*11*).

Influence of the Support

On the basis of the arguments reported so far, we advance an interpretation of our results which is based on the difference in catalytic activity experienced by a mere change in support ($Al_2O_3 \gg SiO_2$). This is related to the nature of the product formed in the interaction of the support with MnO_2 and the amphoteric character of the latter. In an acidic medium Mn^{4+} is easily reduced to Mn^{2+}, a species without any oxidative properties. In alkaline media stable higher oxides are formed with a considerable oxidising power:

$$2MnO_2 + 4OH^- \rightarrow \underset{\text{manganate (IV)}}{2MnO_3^{2-}} + 2H_2O,$$

$$2MnO_2 + 6OH^- + \tfrac{1}{2}O_2 \rightarrow \underset{\text{manganate (V)}}{2MnO_4^{3-}} + 3H_2O,$$

$$2MnO_2 + 4OH^- + O_2 \rightarrow \underset{\text{manganate (VI)}}{2MnO_4^{2-}} + 2H_2O \xrightarrow{\text{oxidn}} \underset{\text{permanganate}}{MnO_4^-}.$$

It is therefore to be expected that besides valence induction, as discussed by Selwood, basic supports such as Al_2O_3 may lead to the formation of other species even though in limited amounts due to the difficult solid–solid interaction. Consequently, the oxidising power of MnO_2 may be enhanced by the action of the support.

It is of interest to notice that $AgMnO_4$ is almost inactive towards CO oxidation, but shows a high activity in the presence of various metallic oxides such as Al_2O_3. These metallic oxides play the role of activators rather than promoters of the heterogeneous reaction between CO and $AgMnO_4$. The MnO_2/γ-Al_2O_3 catalysts have in common with the $AgMnO_4 \cdot MO_x$ reagents (*36*) that essentially no protection from the action of water is required, as opposed to the Hopcalite (MnO_2 +

CuO/Ag_2O) catalysts (*25*). In fact, $AgMnO_4 \cdot MO_x$ reagents exhibit optimum activity at 50% relative humidity at ordinary temperatures. This is quite surprising, especially if we consider that the decomposition reaction of $AgMnO_4$ according to

$$4AgMnO_4 \rightarrow 2Ag_2O + 4MnO_2 + 3O_2$$

is catalysed by adsorbed water (*38*).

From a catalytic point of view, Cu^+ dopants closely resemble the behavior of Ag^+ ions. Nevertheless, the morphology and texture of these sorbents differ considerably with a strong indication of chemical interaction in the former case, clearly shown by TEM (Fig. 7).

ACKNOWLEDGMENT

Thanks are due to Mr. G. Agazzini for taking the electron micrographs.

REFERENCES

1. Grandjean, F., *Bull. Soc. Fr. Mineral.* **33,** 5 (1910).
2. Coolidge, A. S., *J. Amer. Chem. Soc.* **49,** 1949 (1927).
3. Wyart, F., *Bull. Soc. Fr. Mineral.* **56,** 81, 142 (1933).
4. Barrer, R. M., and Woodhead, M., *Trans. Faraday Soc.* **44,** 1001 (1948).
5. Logan, W. R., *J. Appl. Chem.* **16,** 285 (1966).
6. Barrer, R. M., and Whiteman, J. L., *J. Chem. Soc. A,* 19 (1967).
7. Alekseevskii, E. V., and Gol'braikh, Z. E., *J. Gen. Chem. (URSS)* **4,** 936 (1934).
8. Alekseevskii, E. V., *Trans. Mendeleev Congr. 6th* **1,** 245 (1935).
9. Alekseevskii, E. V., and Soskind, A. S., *J. Gen. Chem. (URSS)* **7,** 1638 (1937).
10. Alekseevskii, E. V., and Aleskovskii, V. B., *J. Gen. Chem. (URSS)* **10,** 137 (1940).
11. Alekseevskii, E. V., and Frid, K. V., *J. Gen. Chem. (URSS)* **15,** 3 (1945).
12. Kolthoff, I. M., and Elving, P. J., "Treatise on Analytical Chemistry, II," Vol. 3, p. 231. Interscience, London, 1961.
13. Sandell, E. B., "Colorimetric Determination of Traces of Metals," III, p. 626. Interscience, New York, 1950.
14. Charlot, G., "Les méthodes de la chimie analytique. Analyse quantitative minérale," p. 797. Masson, Paris, 1966.
15. Kuzyatina, N. S., *Zavod. Lab.* **8,** 174 (1939).
16. Nelsen, F. M., and Eggertsen, F. T., *Anal. Chem.* **30,** 1387 (1958).
17. Dalmai-Imelik, J., Leclercq, C., and Mutin, J., *J. Microsc. (Paris)* **20,** 123 (1974).
18. MacKenzie, R. C., "Differential Thermal Analysis," p. 356. Academic Press, New York/London, 1970.
19. Moore, T. E., Ellis, M., and Selwood, P. W., *J. Amer. Chem. Soc.* **72,** 856 (1950).
20. Selwood, P. W., Moore, T. E., Ellis, M., and Wethington, K., *J. Amer. Chem. Soc.* **71,** 693 (1949).
21. Brenet, J., *C.R. Acad. Sci. (Paris)* **247,** 783 (1958).
22. Malati, M. A., *Chem. Ind.,* 446 (1971).
23. Mooi, J., and Selwood, P. W., *J. Amer. Chem. Soc.* **74,** 2461 (1952).
24. Frazer, J. C. W., and Scalione, C. C., U.S. Patent 1,345,323 (1920).
25. Lamb, A. B., Bray, W. C., and Frazer, J. C. W., *Ind. Eng. Chem.* **12,** 213 (1920).
26. Robinson, E., *in* "Proceedings Fifth Iberoamerican Symposium on Catalysis," Lisbon, 1976, p. 103.
27. Kiang, K. D., Li, K., and Rothfus, R. R., *Environ. Sci. Technol.* **10,** 886 (1976).
28. Kanungo, S. B., *J. Catal.* **58,** 419 (1979).
29. Kobayashi, M., Matsumoto, H., and Kobayashi, H., *J. Catal.* **21,** 48 (1971).
30. Kobayashi, M., and Kobayashi, H., *J. Catal.* **27,** 100 (1972).
31. Kobayashi, M., and Kobayashi, H., *J. Catal.* **27,** 108 (1972).
32. Van Den Bosch, P. J. W. M., and De Jong, W. A., *in* "Preparation of Catalysts" (B. Delmon, P. A. Jacobs, and G. Poncelet, Eds.), p. 651. Elsevier, Amsterdam, 1976.
33. Katz, M., *in* "Advances in Catalysis and Related Subjects," Vol. 5, p. 177. Academic Press, New York/London, 1953.
34. Tvarusko, A., *J. Electrochem. Soc.* **111,** 125 (1964).
35. Rushton, H., and Krieger, K. A., *in* "Advances in Catalysis and Related Subjects," Vol. 3, p. 107. Academic Press, New York/London, 1951.
36. Katz, M., and Halpern, S., *Ind. Eng. Chem.* **42,** 345 (1950).
37. Pascal, P., "Nouveau traité de chimie minérale," Vol. XVI. Masson, Paris, 1960.
38. Prout, E. G., and Tompkins, F. C., *Trans. Faraday Soc.* **42,** 468 (1946).